POAC'13
Espoo, Finland

Proceedings of the 22nd International Conference on
Port and Ocean Engineering under Arctic Conditions
June 9-13, 2013
Espoo, Finland

THE COLLISION OF CONE SHAPE ICE SAMPLES AGAINST STEEL PLATES OF VARYING SURFACE ROUGHNESS

Dragt, R.C.[1], Bruneau S.E.[2]
[1] Delft University of Technology, Delft, THE NETHERLANDS
[2] Memorial University of Newfoundland, St. John's, CANADA

ABSTRACT

This paper describes experiments simulating ship collisions with ice, which have been conducted in the laboratory. Polycrystalline, anisotropic ice samples of 259 mm in diameter, at the steel ring/base, were shaped into 30° right angle cones. These cones were driven 40 mm or more into rigid, flat plates of varying roughness. Loads, displacements, spalling quantities and high speed video were recorded for all interactions which were conducted at closing speeds between 0.01 and 100 mm/s at a temperature of -10 °C.

Three circular stainless steel plates were constructed using different contact surface finishes. The smoothest plate was polished to an average roughness (R_a) of 0.13 µm. The sanded medium plate has a roughness of 0.47 µm and the machined rough plate has a surface roughness of 500 µm.

Peak force and cumulative crushing energy were determined at discrete penetrations and plotted against penetration rate and surface roughness. The results indicate that surface roughness influences peak force and crushing energy, though trends vary according to the interaction rate. At low interaction rates, 0.1 mm/s and below, the polished smooth plate gave rise to higher loads than the sanded medium plate. However, at indentation rates of 10 mm/s and above, forces on the medium plate were higher than on the smooth plate. Overall, use of the rough plate resulted in higher forces than both the sanded medium and the polished smooth plate. The data also shows the transition between ductile and brittle behaviour. A discussion of the possible mechanisms giving rise to these results is presented.

KEY WORDS: Ice; Ship; Collision; Crushing; Surface Roughness; Laboratory Experiments;

NOMENCLATURE

α	=	Cone angle [°]	F_p	=	Peak force [N]
A	=	Theoretical contact surface [m^2]	R_A	=	Arithmetic average height
E	=	Crushing energy [J]	Vc	=	Theoretical crushed volume [m^3]
F	=	Force [N]			

1. INTRODUCTION

This paper describes a series of laboratory experiments executed at Memorial University of Newfoundland during the fall of 2012. The experiments are part of the multi-party research program STePS^2 (Sustainable Technology for Polar Ships and Structures) and are a continuation of earlier work done within the project (Bruneau et al., 2012; Dillenburg, 2012). The earlier work involved experiments that simulated small-scale ship-ice collisions in which indentation rate, ice temperature, ice type, and cone slope were varied. This paper describes follow-on experimental work investigating the influence of structural surface roughness on similar collision experiments.

2. EXPERIMENT SET UP

Figure 1 illustrates the experimental set up whereby an ice sample in a steel ice holder is secured to a hydraulic actuator which, when triggered, moves vertically at a constant rate crushing the ice into a crushing plate affixed to a load cell. The whole set up is stationed inside a cold room, where the temperature was fixed at -10° C.

Both the load cell and the hydraulic actuator are controlled using a computer, placed outside the cold room. High speed video footage of the ice crushing is made through a window in the cold room.

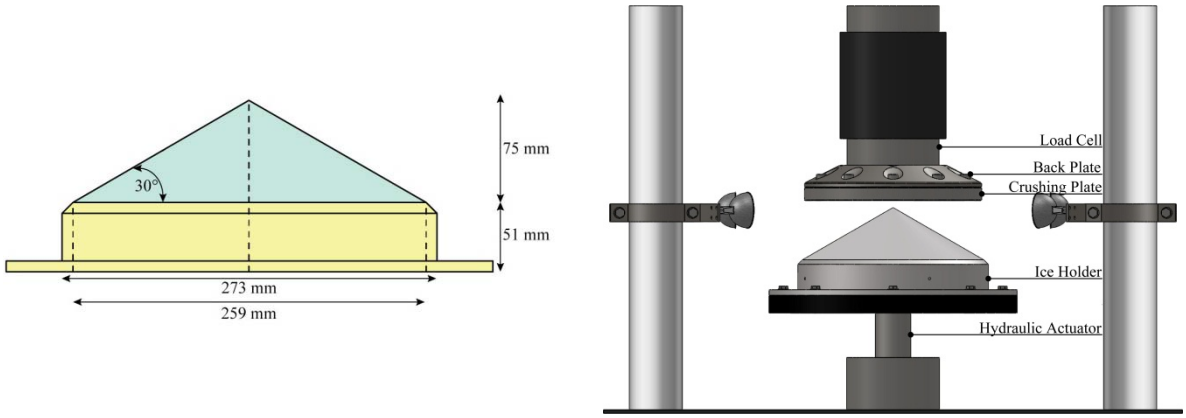

Figure 1. Schematics of the ice and ice holder (left) and the test set up prior to testing (right).

2.1. Ice Samples

The preparation method for the ice samples used for crushing is documented in earlier work (Bruneau et al., 2012; Dillenburg, 2012). The production method established was relatively simple, with the primary objective being the production of samples with a consistent, reproducible set of mechanical properties, and internal structure, which were also a reasonable facsimile of natural ice that is polycrystalline and anisotropic.

In summary, the process involves the unidirectional freezing of seeded water in an over-sized container. The ice seeds are obtained from mechanically crushed commercial ice cubes and are carefully sieved to control the grain size in the range [4 – 10^{+} mm]. The particle size distribution of the seeds is provided in Figure 2 and a cross-polarized view of a thin section of sample ice is shown in Figure 3. The seeds are then placed inside moulds, thoroughly shaken to compact them and topped off with distilled, deionized and degassed water, chilled to approximately 0° C.

Figure 4 is a photograph of an ice mould/container filled with ice seeds prior to adding water. This represents one of eight moulds, which are accommodated simultaneously in

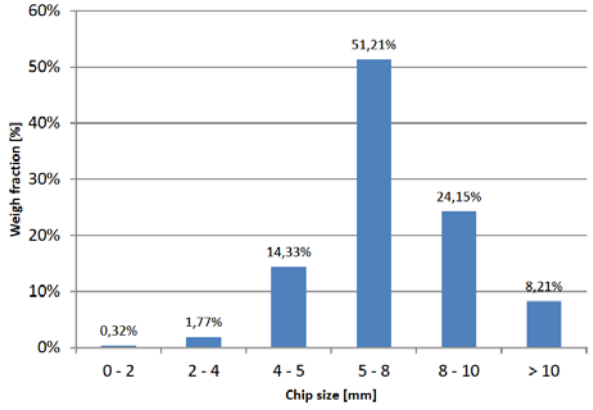

Figure 2. Size distribution for the seeding.

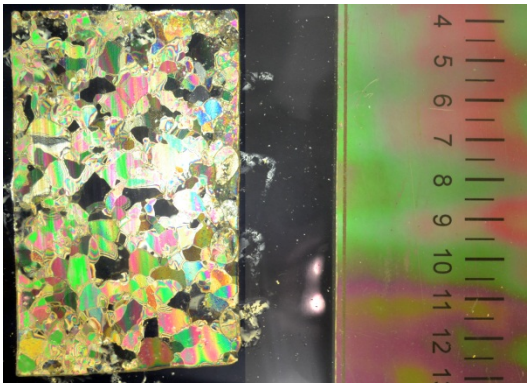

Figure 3. Vertical thin section of an uncrushed sample. Scale is in cm.

customized -25° C chest freezers. Figure 5 is a schematic of the freezer set-up, which resulted in uniform, uncracked cylindrical ice blocks rigidly embedded in steel support rings.

Ice samples thus grown are further shaped into smooth sharp cones using a customized rotary ice shaver. The machine rotates at 300 rpm and is analogous to a combined pottery wheel and lathe, making use of commercially available planar blades as cutting tools. The edges of the steel ring-holders are bevelled at 45° to make sure the ice can be machined in a conical shape and four small steel lugs extend radially inward from the ring and are thus embedded in the ice to secure samples during handling and machining. The result is an ice cone with a base diameter of 259 mm, a slope of 30° and a total height of 126 mm, of which 51 mm is located inside of the ice holder leaving 75 mm exposed. Evidently, samples procured in this manner have minimal internal stresses according to work by Cole (1984) on the freezing process and as long as the planer blade is sufficiently sharp, the machining does not influence the internal structure of the ice (Lieu & Mote, 1984). Finally, the samples are covered and placed inside the cold room for at least one day prior to testing to allow temperature relaxation (Jones et al., 2003).

Figure 4. Bucket filled with chips.

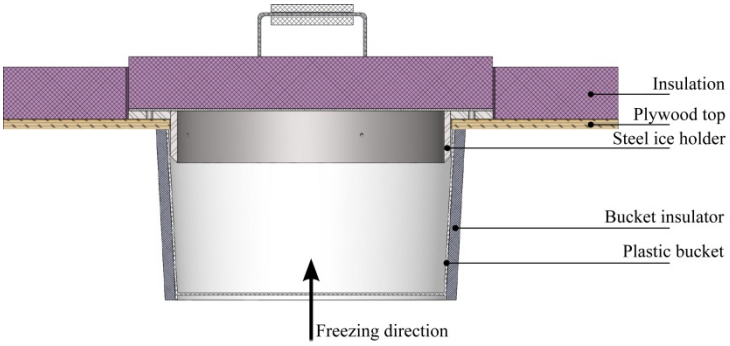

Figure 5. Schematic view of the freezing set-up.

2.2. Crushing Plate

The crushing surface consists of two parts, a stainless steel crushing plate and a steel back plate. The crushing plate, made out of ¾ inch stainless steel, is the contacting surface and is, therefore, carefully prepared and handled. It is bolted to the back plate, which connects to the load cell and provides for enough stiffness to avoid vibrations in the system (Dillenburg, 2012).

In total, three different crushing plates were used for these experiments. The surface roughness of these plates is characterized as *smooth*, *medium* and *rough*. The *smooth plate* was given a mirror surface finish using fine polishing cloths. Measurement of the arithmetic average roughness height R_A[1] gives an average value of 0.13 µm with the roughness pattern being one of barely visible concentric rings resulting from the machining and polishing process. The medium plate is the same one used in earlier experiments (Dillenburg, 2012) and was determined to have an R_A of 0.47 µm also with a concentric roughness pattern. The *rough plate* was designed with a R_A of 500 µm. To achieve this, groves were machined into the steel plate in intersecting longitudinal and transverse (perpendicular) directions. Thus the noticeably rough surface had a square pattern unlike the much smoother concentric circular patterns of the other plates. All three crushing plates, and their schematic roughnesses, are shown in Figure 6. Comparing the surface roughnesses to material values shows that the

[1]Mathematical definition of the arithmetic average height $R_A = \frac{1}{l}\int_0^l |y(x)|dx$ (Gadelmawla et al., 2002)

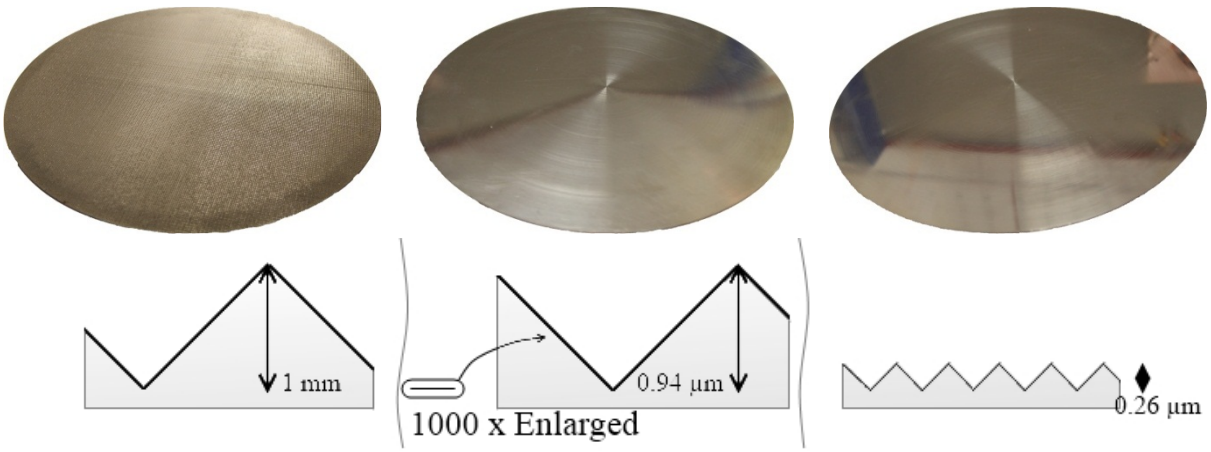

Figure 6. The rough (left), medium (middle) and smooth (right) crushing plate with a schematic comparison of their roughnesses.

smooth plate is comparable to painted steel. The medium plate has a roughness comparable to scored steel and the rough plate compares to rough concrete (Saeki et al., 1964).

2.3. Test Plan

The two dependant variables in the test plan were indentation rate and surface roughness. Best efforts were made to reproduce precisely all other important test factors including sample manufacturing materials and techniques, handling and execution, test temperature, DQ settings and equipment, etc. The tests were performed at five different speeds, which evidently and unambiguously spanned the ductile, transitional and brittle range of material behaviour (Dillenburg, 2012): 0.01 mm/s, 0.1 mm/s, 1 mm/s, 10 mm/s and 100 mm/s. This range was essentially bounded by the limits of the laboratory hydraulic system, thus rates beyond this were not experimentally possible.

For improved statistical significance and for experimental rigor all tests were repeated at least twice, typically three times as is shown in the test matrix below (Table 1).

Table 1. Test matrix with changing (and non-changing) variables and number of runs.

Plate Roughness:	**Indentation Speed [mm/s]:**				
	0.01	***0.1***	***1***	***10***	***100***
R_A = *0.13 µm*	3	3	3	3	3
R_A = *0.47 µm*	2	2	2	2	2
R_A = *500 µm*	3	3	3	3	3

Non-Changing Variables:	
~ Temperature:	-10° C
~ Grain Size	4 – 10^+ mm
~ Cone angle:	30°

Sampling frequency (and equipment response rates) exceeded 2000 Hz for load, displacement and high speed imaging. Sample weight was measured prior to and after testing to account for spalled material volumes, and, thin section samples were sawn from the remaining ice after each test. Photos were taken of the samples prior to after testing, including images of the crushed ice adhered to the crushing plate.

3. ANALYSIS

3.1. Force and Nominal Pressure

The forces are plotted as a function of indentation from the point of first contact between ice and crushing plate. The peak force F_p is defined as the maximum force at a given time interval. The nominal pressure p is calculated by dividing the force by the theoretical circular contact surface, a function of indentation x, as shown in Equation 1, in which α is the cone angle of 30°. It is understood that this is an expedient approximation in the absence of

measured data, as the instantaneous area of ice contact with the plate deviates from the theoretical contact area due to spalling and other complex material behaviour.

$$p(x) = \frac{F(x)}{A(x)} \qquad \text{with} \quad A(x) = \pi \left(\frac{x}{\tan \alpha}\right)^2 \tag{1}$$

3.2. Energy

The crushing energy E, calculated using the trapezoid integration method, is shown as Equation 2. The integral is made over the maximum common indentation between samples.

$$E = \int_0^{x_{max}} F(x)dx \approx \frac{1}{2}\sum_{i=1}^{N}(x_i - x_{i-1})\big(F(x_1) + F(x_{i-1})\big) \tag{2}$$

3.3. Spalling Behaviour

The spalling behaviour is measured by weighting the sample before and after the testing. To compensate for the difference in maximal indentation, the weight of the spalls is divided by the theoretical crushed volume V_c (see Equation 3).

$$V_c(x_{max}) = \frac{1}{3}\frac{\pi x_{max}^3}{\tan^2 \alpha} \tag{3}$$

4. RESULTS

4.1. Force Curves, Nominal Pressures and Spalling

Figure 7 shows an example of the force measured on the medium roughness crushing plate at all five indentation rates. Figure 8 shows the corresponding nominal pressures. Due to the very small initial contact area, the nominal pressure spikes just after initial contact.

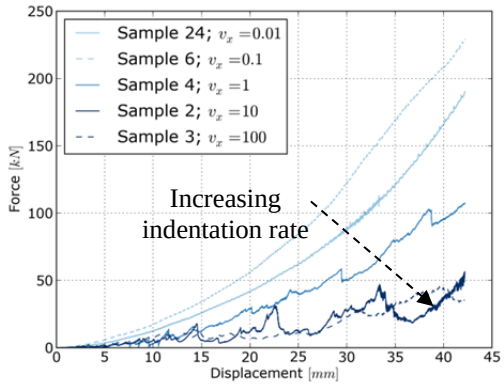

Figure 7. Force curves measured with the medium crushing plate.

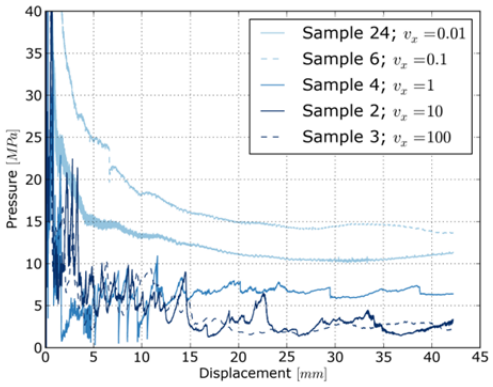

Figure 8. Nominal pressures, calculated using the theoretical contact area.

Figure 9 shows two sets of frame shots from the same samples, at two indentations (22 mm and 37 mm). Table 2 shows the main parameters (indentation rate, peak force, nominal pressure at peak force, indentation at peak force and spall weight) for each of the five samples described above. Note that the value for the peak force is highly dependent on the interval taken. This is seen at Sample 03, where the peak force is not located at the end of the interval.

4.1.1. Indentation rate effects

The effect of indentation rate on the mechanical ice behaviour is clearly visible. At low indentation rates, *0.01* and *0.1 mm/s*, the ice shows ductile behaviour, resulting in relatively

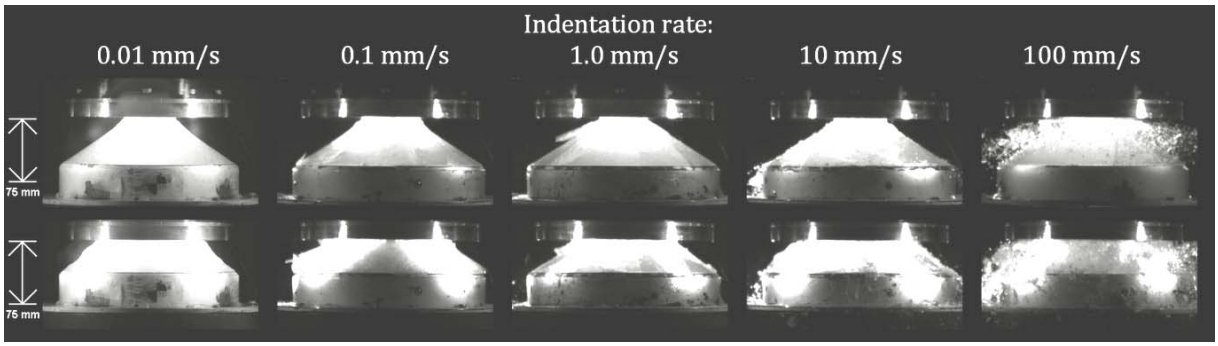

Figure 9. Pictures of crushing tests at five speeds on the medium crushing plate, synchronised on indentation (**above:** 22 mm indentation, **below:** 37 mm indentation).

Table 2. Parameters from ice crushing tests on medium plate for five samples. The weight of a sample (excluding steel holder) is about 3.6 kg.

	v_x [mm/s]	Peak Force [kN]	Nominal Pressure at Peak Force [MPa]	Indentation at Peak Force [mm]	Spall weight [g]
Sample 24	0.01	165.8	11.34	42.20	24
Sample 06	0.1	208.2	13.66	42.20	116
Sample 04	1	103.0	6.41	42.20	509
Sample 02	10	47.0	3.37	42.20	719
Sample 03	100	45.3	3.07	39.56	499

high forces and little spalling. The force and pressure curves are smooth, which means there is no major stress relieve due to cracks and spalling events.

At intermediate speed, *1 mm/s*, the ice behaviour is classified as ductile-to-brittle. Although more cracks are apparent in the sample, as can be seen in the snap shots and the stress relieve in the force curve, the samples still has a force build-up. However, the amount of spalling increases as well.

Finally, at high crushing rates, *10* and *100 mm/s*, the ice behaves as a brittle solid. Large cracks form during the test, relieving stress in a saw tooth motion and creating many spalls. After a stress relieve event, it takes some indentation before the force builds up again. Keep in mind that these samples are indentation at a high rate, giving the ice little time to settle.

4.1.2. Indentation effects at different surface roughnesses

The examples above are all taken from tests on the medium crushing plate. Evidently, the general trends with respect to indentation rate effects are the same for the three different roughnesses. This is seen in Figure 10 and Figure 11 where five indentation speeds are plotted for the smooth and the rough crushing plate.

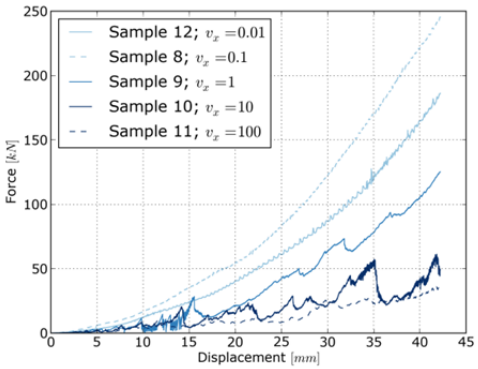

Figure 10. Force curves for the smooth plate.

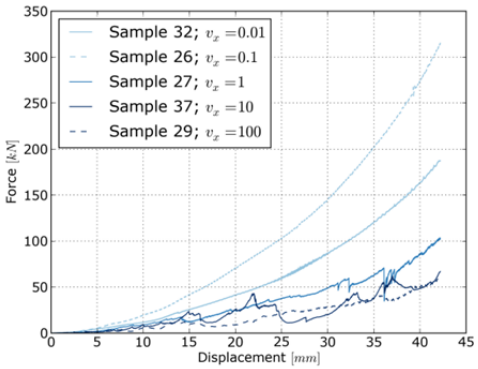

Figure 11. Force curves for the rough plate.

4.2. Peak Force and Crushing Energy

The effect of surface roughness on the crushing forces is better visualised by plotting the average values and normalized sample standard deviations (Figure 12 and Figure 13). The relative difference between the plates (in terms of peak force and crushing energy) is plotted in Figure 14 and Figure 15 by normalizing the data with respect to the medium crushing plate.

At the lowest indentation rate, *0.01 mm/s*, the peak forces are close together. However, the spread in values is also very low and the force traces are divergent, enlarging the gap between the plates at higher indentations.

At an indentation rate of *0.1 mm/s*, the highest forces are observed. The differences between the crushing plates are clearly distinguishable, due to the low spread of data points. The highest forces are measured on the rough plate. Note that not the smooth but the medium crushing plate provides the lowest forces. The same trend is seen in the crushing energy.

The intermediate speed, *1 mm/s*, the ice shows ductile-to-brittle behaviour. Both the peak force and the crushing energy of the medium and the smooth plate show little difference. The rough plate, however, still shows higher crushing energies and forces.

The peak force for the rough crushing plate, at *10 mm/s* indentation, is much higher than the peak force for the medium and smooth plate, which are again quite alike. Looking at the crushing energy, the smooth plate gives a slightly higher energy than the medium plate while the rough plate has the largest relative difference with the other two.

At the highest indentation rate, *100 mm/s*, the smooth plate gives the lowest peak force and energy, the rough plate the highest and the medium plate is in the middle. The standard deviation of the values is for each crushing plate low, resulting in nicely ordered data points.

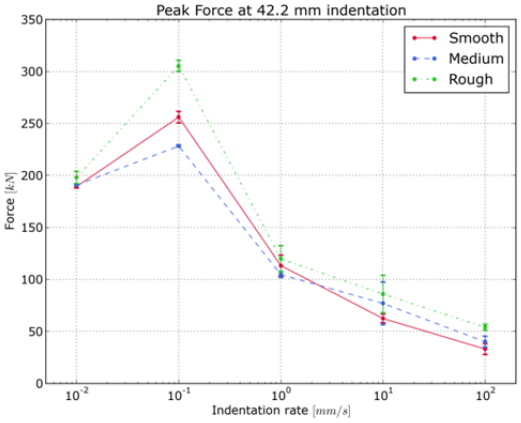

Figure 12. Peak Force.

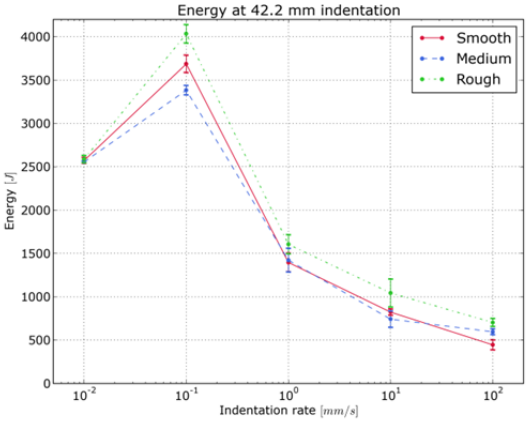

Figure 13. Crushing energy.

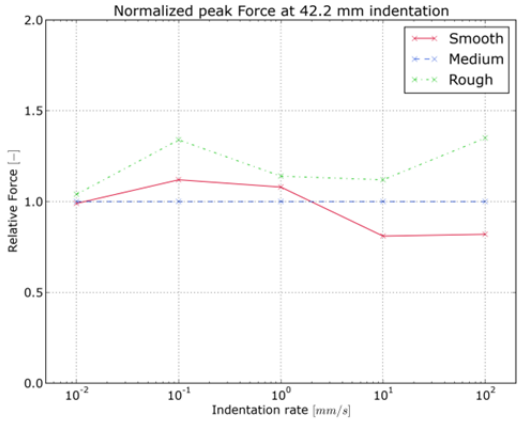

Figure 14. Peak force normalized at the medium crushing plate.

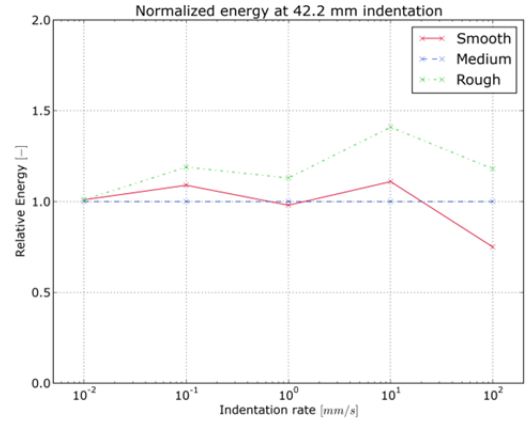

Figure 15. Crushing energy normalized at the medium crushing plate.

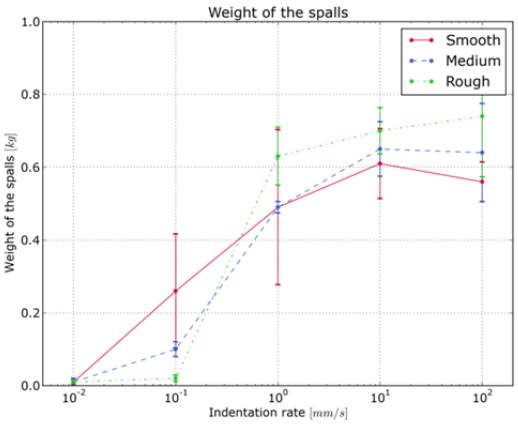

Figure 16. Spall weight; notice the large spread in values.

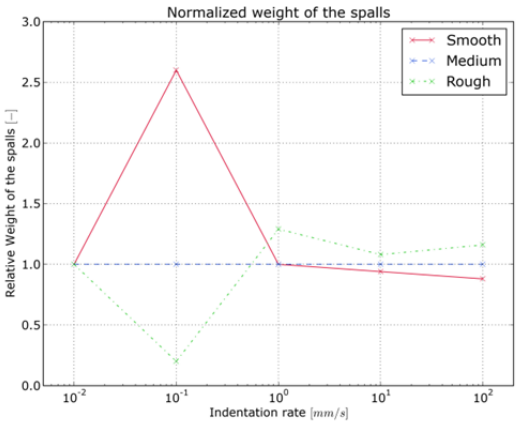

Figure 17. Normalized spall weight with respect to the medium crushing plate.

4.3. Spalling behaviour

Figure 16 and Figure 17 show the spall weight and the normalized spall weight. In general, more spalling is observed at higher crushing velocities, which is in agreement with the brittle material behaviour. Furthermore, the spread in values is quite large due to randomness associated with spalling.

In general, the medium plate induces the most spalling, except at 0.1 mm/s, where the smooth plate has a peak in spall weight. This is most likely due to a single large spall at one of the tests.

4.4. Adhesion

After crushing, photos are made of the crushing plate, showing ice being stuck to the plate after the sample itself is retracted (directly after the test is completed). These photos are shown in Table 3. From this table is seen that the large amounts of ice stuck to the smooth plate while almost no ice stuck to the rough plate. Noteworthy is that it also took much more effort to clean the ice from the smooth plate than from the other ones.

Table 3. Crushing plates after testing.

Rough-ness	**Indentation speed**				
	0.01 mm/s	*0.1 mm/s*	*1 mm/s*	*10 mm/s*	*100 mm/s*
Smooth plate					
Medium plate					
Rough plate					

5. DISCUSSION

Friction is described by Barnes et al. (1971) as the sum of two components, namely ploughing and adhesion. These two effects can be used to explain the behaviour seen, although these experiments are not designed to single out a single effect.

5.1.1. Ploughing

Ploughing is initiated by the relatively hard surface profile asperities penetrating into the softer ice. This leads to an increased strain rate in the extruding ice. Due to the viscoplasticity, this results in an increase in tangential stress, which increases friction (Fiorio et al., 2002). This behaviour is responsible for a higher confinement in the sample when crushed against

the rough plate, resulting in higher crushing forces. Furthermore, as spalling initiation occurs at shear zones with low confining pressure (Zou et al., 1996), this reduces spalling.

Both these effects, in increased force / crushing energy and low spalling at the rough plate, are observed in the experiments. Nevertheless, this also states that the forces on the medium plate should be higher than on the smooth plate, which is not uniformly the case.

5.1.2. Adhesion

On contact, steel and ice form an adhesive bond which takes a certain amount of force to break. If the adhesive bond is stronger than the cohesive bond within the ice, the ice will stick to the plate and shear internally. This effect is seen on the crushing plate after retracting the sample. Hereby, a stronger bond is observed between the ice and the smooth plate than between the ice and medium or rough plate.

In his work, Barnes et al. (1971) elaborate on the real and apparent contact area between two surfaces. Although the apparent contact area is higher on the rough plate, the real contact area may well be smaller, as ice fills the openings between the asperities, as is shown in Figure 18. This might enable the ice to form a stronger adhesive bond with the steel, as there are more points of contact.

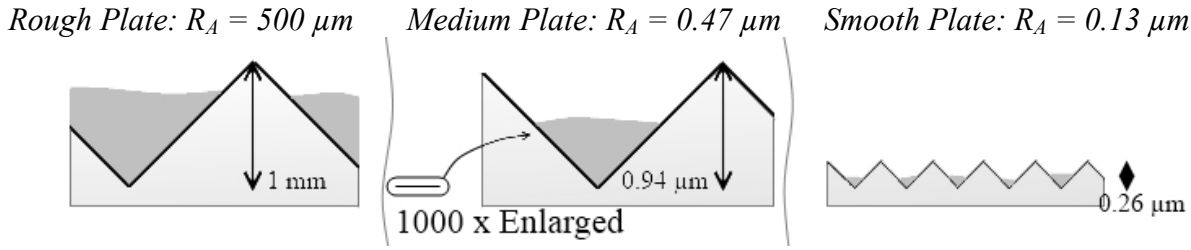

Figure 18. Schematic overview of the apparent and real area of contact at the rough (left), medium (middle) and smooth (right) crushing plate. The dark grey area is ice in between the asperities, lowering the real area of contact.

5.1.3. Rate dependency

At low indentation rates, the differences between the medium and smooth plate are more apparent than at high indentation rates. Also, there is more spalling to be seen at higher rates. As, with increasing crushing speed, the ice has less time to relocate and settle, there is less confinement, resulting in lower forces and more spalling, hence the brittle solid-like behaviour.

At these high indentation rates, the force build up and release happens in a saw tooth motion, especially at 10 mm/s. Also, the difference in adhesive force on the crushing plate is less apparent as at low crushing rates. This could point to an increased importance of the ploughing effects on friction.

5.1.4. Experiment design

The experiments, done in this fashion, are only suitable to recognize the general trends and effects of surface roughness. Dedicated follow-up tests are necessary to single out the various effects (like friction coefficients and adhesion factors) and investigate their individual influences on the crushing forces.

6. CONCLUSIONS AND RECOMMENDATIONS

The experiments performed clearly show rate and surface roughness dependency on ice indentation loads. At slow indentation speeds, 0.01 and 0.1 mm/s, the ice behaves in a ductile fashion, resulting in a low spall weight and high indentation forces. The rough plate induces

the highest forces at both speeds. At 0.1 mm/s the highest forces are measured. Noteworthy at this rate are the forces on the smooth plate, which are higher than at the medium plate. This effect is explained by an increased adhesion bond due to a larger real contact area.

At higher speeds, the ice starts to behave in a brittle fashion, resulting in more spalling. Also, the force build-up happens in a saw tooth fashion and the difference between the smooth and medium plate is less apparent. Finally, at the highest speeds, lower forces are measured on the smooth plate instead of the medium plate.

In general, these experiments show that a rougher surface will induce higher forces. However, a really smooth plate will not always reduce the indentation force.

6.1. Recommendations

These tests show a clear dependency on surface roughness, but are not designed to measure friction or single out any other particular. Therefore, it is recommended to execute friction related experiments on the crushing plates, to determine their coefficient of friction. This way, the results are more comparable with existing tests, described in literature.

ACKNOWLEDGEMENTS

The authors would like to thank the STePS^2 research project and her partners for making this research possible. Special thanks are given to Craig Mitchell for assistance and advice in conducting the experiments and to Andrew Manuel for the hands-on laboratory work.

REFERENCES

Bruneau, S.E. and Dillenburg, A.K. and Ritter, S., 2012, Ice sample production techniques and indentation tests for laboratory experiments simulating ship collisions with ice, *ISOPE2012*.

Barnes, P. and Tabor, D. and Walker, J., 1971, The friction and creep of polycrystalline ice, *Proceedings of the Royal Society A*, vol. 324, p. 127-155

Cole, D.M., 1979, Preparation of polycrystalline ice specimens for laboratory experiments, *Cold Regions Science and Technology*, vol.1, p. 153-159.

Dillenburg, A.K., 2012, 'Rate dependency in conical ice indenter failure', Master's Thesis, University of Duisburg-Essen, Institute of Ship Technology, Ocean Engineering and Transport Systems.

Fiorio, B. and Meyssonnier, J. and Boulon, M., 2002, Experimental study of the friction on ice over concrete under simplified ice-structure interaction conditions, *Canadian Journal of Civil Engineering*, vol. 359, p. 348-359

Gadelmawla, E.S. and Koura, M.M. and Maksoud, T.M.A. and Elewa I.M. and Soliman, 2002, H.H., Roughness Parameters, *Journal of Materials Processing Technology*, vol. 123, p. 133-145

Jones, S.J. and Gagnon, R.E. and Derradji, A. Bugden, A., 2003, Compressive strength of iceberg ice, *Canadian Journal of Physics*, vol. 81, p. 191-200.

Lieu, D.K. and Mote, C.D. Jr., 1984, Experiments in the machining of ice at negative rake angles, *Journal of Glaciology*, vol. 30.

Saeki, H. and Ono, T. and Nakazawa, N. and Sakai, M. and Tanaka, S., 1964, The coefficient of friction between sea ice and various materials used in offshore structures, *Offshore Technology Conference*.

Zou, B. and Xiao, J. and Jordaan, I.J., 1996, Ice fracture and spalling in ice-structure interaction, *Cold Regions Science and Technology,* vol. 24, p. 213-220